

vehicle exhaust. The average mass concentration of NO_2 was $73.1 \mu\text{g m}^{-3}$, which is much higher than that of SO_2 ($9.8 \mu\text{g m}^{-3}$). O_3 was a product of the photochemical reaction between nitrogen oxides (NO_x) and volatile organic compounds (VOCs). High concentrations of NO_2 resulted in a high concentration of O_3 . However, O_3 remained at a low level during the fourth episode, especially on 30 and 31 October, whereas $\text{PM}_{2.5}$ and other gaseous pollutants reached their peaks at this time, which indicated that the photochemical reaction during the fourth episode was not strong and that heterogeneous reactions play a major role in the haze formation in the fourth episode. All of the gaseous pollutants showed daily variation and reached a maximum on 18 October. These were also related to the variance in the height of the PBL, which will be discussed in Sect. 3.2.4.

Like the other severe hazes (Tao et al., 2014a, b) in last two years, the haze in October 2014 also influenced China to a large extent (Fig. 4). According to the $\text{PM}_{2.5}$ spatial distribution over China, the haze originated from the Northern China Plain (NCP) and developed to the southwest and northeast directions. A similar situation occurred in September 2011, when the haze originated from Beijing and developed in the same directions (Liu et al., 2013a). Moreover, the haze influenced a large area of Middle China and Northeast China; for example, the concentration of $\text{PM}_{2.5}$ in Harbin, which is a large city in Northeast China, peaked at $664 \mu\text{g m}^{-3}$ during the third haze episode.

3.1.2 Optical properties

The temporal variation of the aerosol scattering at ambient environment coefficient b_{sp} (RH), the absorption by NO_2 coefficient b_{ag} , the aerosol absorption coefficient b_{ap} , the atmospheric extinction at ambient environment coefficient b_{ext} (RH) and the SSA are shown in Fig. 5. Data for b_{ext} (RH) were complete for the whole observation period, whereas the other three parameters were not available until 15 October. With clear diurnal variation, b_{sp} , b_{ap} and b_{ext} increased day by day during the haze episodes and decreased sharply at the end of these haze episodes. Because b_{sp} (RH) was calculated

10995

using b_{ap} and b_{ext} and because b_{ap} was relatively small compared to b_{ext} , the b_{sp} (RH) had nearly the same temporal variation as b_{ext} . The maximum b_{ext} was 5611 Mm^{-1} at 22:00 LST on 25 October, and the average b_{ext} reached 1069 Mm^{-1} . Both data were much higher than those of other studies (Garland et al., 2008; Jung et al., 2009). The SSA in Fig. 5 was calculated using the aerosol extinction at ambient environment coefficient, b_{sp} (RH). Aerosol representing fresh emission always has a low SSA, whereas aged aerosol has a higher SSA (Garland et al., 2008). As a result, the SSA showed an increasing trend during the haze episodes. Four sudden decreases in the SSA were observed during the dawn of 16, 22, and 26 October and 1 November. The first two decreases occurred at the beginning of haze episodes, which represented large quantities of freshly emitted aerosol. Because local emissions in Beijing showed a steadier pattern, the sudden change in SSA indicated pollutant transport from the vicinity of Beijing (discussed in Sect. 3.2.2). The other two decreases occurred at the end of haze episodes when strong winds blew over Beijing and the pollutants were largely removed (discussed in Sect. 3.2.3). Aged aerosol was cleared and new aerosols increased in a short time (Guo et al., 2014). Thus, SSA decreased sharply.

3.2 Formation mechanism of haze episodes

3.2.1 Secondary transformation of aerosols

Water-soluble ions are a primary component of aerosols and play a major role in the hygroscopic growth of aerosols. The temporal variation of major components (organic matter, SO_4^{2-} , NO_3^- , NH_4^+ , Cl^- and black carbon (BC)) in PM_1 is shown in Fig. 6. Organic matter contributed most to the PM_1 , followed by NO_3^- , SO_4^{2-} , NH_4^+ , BC and Cl^- . The mass concentration of SO_4^{2-} was always higher than that of NO_3^- , especially in the winter time, when the heat supply is prevalent in North China (Zhao et al., 2013). Although Beijing is replacing coal with natural gas for a heat supply, the influence from the vicinity is still enormous. However, in this study, the mass concentration of NO_3^-

10996

was always higher than that of SO_4^{2-} . The concentration of NO_3^- , which was primarily transferred from NO_x , represented the contribution of motor vehicle sources. The heat supply is not available during October in NCP, and the motor vehicles remained at a similar level throughout the year, which implied that motor vehicles played a more important part in the hazes in the autumn. During the haze periods, the percentage of NO_3^- and NH_4^+ increased, whereas the percentage of organic matter continued to decrease. When strong wind blew pollutants away, the percentage of organic matter increased sharply. On the contrary, the percentage of NO_3^- decreased in a short time and did not return for a certain time. SO_4^{2-} varied similarly to NO_3^- but in a much milder pattern. After the strong wind, even the concentration of SO_4^{2-} decreased, and the return-back time was much shorter than that of NO_3^- . This indicates that even though the concentration of SO_4^{2-} was lower than that of NO_3^- , the oxidation rate from SO_2 to SO_4^{2-} was faster. It has been reported that the existence of high levels of NO_x may accelerate the reaction from SO_2 to SO_4^{2-} (He et al., 2014).

Even though all of the components in PM_{10} increased during the haze events, the accumulation pattern might be different for each component. Comparatively, the increasing pattern of SNA (SO_4^{2-} , NO_3^- and NH_4^+) was likely from local emissions. Diurnal variation of the concentration of SNA also existed, but it was not as significant as that of organic matter, Cl^- and BC. There is also no sudden increase in the concentrations of SNA. They were more likely to accumulate stably with high RH and a stagnant atmosphere. When the RH was high and the atmosphere was stable, gases such as SO_2 and NO_x transform to SNA at a fast rate. A clear increase in the SNA percentage can be seen in the pie charts in Fig. 6. The values for SO_4^{2-} , NO_3^- and NH_4^+ in PM_{10} increased from 8.48, 20.55 and 9.46 % in the non-haze period to 12.7, 27.5 and 12.14 % in the haze episode, respectively. Continuous increasing of SNA indicated that the formation of new SNA during the haze episodes contributes most of the formation of the haze. During the hazes in January 2013, high conversion from the gas phase of SO_2 and NO_x to the particle phase of SO_4^{2-} and NO_3^- was found, and heterogeneous forma-

10997

tion of SO_4^{2-} and NO_3^- was considered to be important, especially during low visibility episodes (Quan et al., 2014).

SOR and NOR were important factors, showing that gaseous species would be oxidized to secondary aerosols in the atmosphere (Sun et al., 2006). They are widely used in the analysis of the secondary transformation of aerosols. The temporal variations of SOR and NOR are shown in Fig. 7. SOR was mostly higher than 0.2, and NOR was mostly higher than 0.1, indicating intense secondary formation of SO_4^{2-} and NO_3^- (Fu et al., 2008). SOR and NOR increased during the haze episodes with accumulated pollutants. Furthermore, SOR increased more quickly than NOR. To compare the rate of increase of SOR and NOR, the slope of the SOR and NOR in the observed haze are calculated. To reduce the influence of the diurnal variation of SOR and NOR, the first and last peak values in the figure are chosen in the calculation. Thus, the slope r is:

$$r(\text{SOR}, \text{h}^{-1}) = \frac{\text{SOR}_{\text{max}} - \text{SOR}_{\text{min}}}{T(\text{h})} \quad (7)$$

$$r(\text{NOR}, \text{h}^{-1}) = \frac{\text{NOR}_{\text{max}} - \text{NOR}_{\text{min}}}{T(\text{h})} \quad (8)$$

The results are shown in Table 3.

In the three observed haze episodes, $r(\text{SOR})$ is 3.4, 1.6, and 4.2 times $r(\text{NOR})$, which indicated faster production of SO_4^{2-} , even though the concentration of SO_4^{2-} was lower than that of NO_3^- . Meanwhile, after the strong wind, which decreased SOR and NOR sharply, low SOR still existed, whereas NOR was nearly 0. These findings explained the shorter return time of SO_4^{2-} after the haze episodes.

3.2.2 Combustion of biomass and regional transport

Biomass burning became prevalent in NCP during the autumn harvest. The combustion was primarily conducted in the open field. Pollutants, such as BC and CO, were emitted on a large scale and influenced the air quality not only in the emission region but also

10998

in the downstream city. Hence, biomass burning in the surrounding provinces was an important cause of the hazes in the autumn in Beijing. Fire points in China, based on data from MODIS Terra and Aqua satellites, on 6 October are shown in Fig. 8a. On 6 October, 267 fire points were found in China, among which 29, 163 and 30 fire points were found in Hebei, Henan and Shandong provinces, respectively. In total, 1957 fire points, which were caused by biomass burning in the whole of October, were found in China, among which 54, 26 and 57 fire points were found in Hebei, Henan and Shandong provinces, respectively. Although the fire points were more strictly controlled in 2014 compared to 2013, the influence of biomass burning still could not be neglected.

The backward trajectories of Beijing during the first haze episode reflect how the biomass burning influenced Beijing (Fig. 8b). A total of 9 backward trajectories of 48 h were drawn with the HYSPLIT model online version. The backward trajectories started from 17:00 LST on 11 October and restarted a new trajectory every 12 h. The air mass during the first haze episode mainly came from the south and southeast, originating from Hebei, Henan, Shandong and even Anhui Province. The pollutants from biomass burning in these provinces were transported to Beijing. Once the meteorological conditions were stagnant, haze formed and was aggravated in this region. A similar situation occurred in the haze in 2007 (Li et al., 2010). Therefore, biomass burning is a tough challenge for air pollution control in the autumn.

Based on the temporal variation of each component in Fig. 6, the organic matter, Cl^- and BC had similar variation patterns. In addition to clear diurnal variations, which were caused by the diurnal development of PBL, a sudden increase in the concentration before each haze period was found for the organic matter, Cl^- and BC. On 18 October, the height of the PBL (468.7 m) was 21.1 % higher than that on 17 October (386.9 m), but the concentrations of organic matter, Cl^- and BC were 6, 6 and 4 times the values of the day before. Organic matter, Cl^- and BC were emitted from biomass burning; abnormal high values and a sudden increase in organic matter, Cl^- and BC indicated spatial transport of pollutants from straw burning. Consequently, regional pol-

10999

lutant transport was important for haze formation in October 2014, and straw burning was a significant pollution source.

3.2.3 Stationary synoptic condition

Pressure systems can influence the wind and precipitation of a region. Surface weather maps of East Asia at 02:00 LST on 7~10 October during the first haze episode are shown in Fig. 9. The NCP was dominated by a weak high-pressure system on 7 October, which lasted for the next two days. The weak high-pressure system resulted in low surface wind and relatively stagnant weather, which was unfavorable for the dispersion of air pollutants. The high-pressure system slowly moved towards the northeast. Meanwhile, the Mongolia anticyclone (a low-pressure system) moved towards and encountered the high-pressure system on 9 October, which brought wind and caused a small decrease in $\text{PM}_{2.5}$ on the dawn of 9 October. However, the weak high-pressure system dominated the NCP on 10 October, and the weather became stagnant again until 11 October, when another strong Mongolia anticyclone moved to the NCP, and the first haze episode ended.

The wind fields at 02:00 LST on 10, 20, 24, and 31 October in the NCP region are shown in Fig. 10, representing typical days in the four haze episodes. Generally, the wind speeds are slow during the haze episodes. In addition, the wind slowed sharply around Beijing city in all four figures. For example, on 31 October, the wind over the NCP came east from the Bohai Sea. The wind separated into two directions when it encountered Beijing, one blowing to the north and the other blowing to the south. The wind over Beijing maintained a low speed. A similar phenomenon was observed in January 2013 when a severe haze occurred in Beijing (Tao et al., 2014b). Moreover, the wind on 10 October was smooth, blowing from the southeast of Beijing and then turning to the northeast. The wind around Beijing was clearly slowed and became strong after blowing over Beijing. The city acted as a large obstacle for the wind, slowing the wind speed, disturbing the wind direction and affecting other properties of the wind (Miao et al., 2009). The wind on 20 October was more complex. Winds from the southwest

11000

The relationships between RH and SOR and between RH and NOR are illustrated in Fig. 13. SOR and NOR were highly correlated with RH. The correlation coefficients of SOR and NOR with RH are 0.79 and 0.55, respectively, which are much higher than those in a previous study (Han et al., 2014), indicating the particularly high importance of RH during the haze episodes in this study. SOR reached a minimum when RH was approximately 40%. When RH was > 40%, SOR increased with increasing RH, whereas SOR decreased with increasing RH when RH was < 40%. The conversion from SO₂ to SO₄²⁻ requires water vapor as a reactant. Hence, when RH was > 40%, the high RH became a major factor accelerating the production of SO₄²⁻. The conversion is an endothermic reaction, which indicates that high temperature can promote the conversion. RH and temperature have an inverse correlation. When the RH was lower than 40%, water was not adequate to accelerate the conversion. As a result, the temperature became the most important factor in the reaction. Therefore, when the RH was lower than 40%, SOR decreased with decreasing temperature but not with increasing RH. The formation of NO₃⁻ is more complex than that of SO₄²⁻, so the correlation of NOR and RH was much weaker than that of SOR and RH. However, a clear positive correlation was still observed. No minimum value was found for NOR, and high RH can promote NOR.

The measured $f(\text{RH})$ values at ambient RH during the observed period are depicted in Fig. 14. The curve is similar to those of other studies, indicating an increasing tendency of $f(\text{RH})$ with increasing RH. Usually, the exponential relationship between $f(\text{RH})$ and RH can be fitted by an empirical function: $f(\text{RH}) = 1 + a(\text{RH}/100)^b$. In this study, the curve fitting parameters a and b were 3.79 and 6.10, respectively. $f(\text{RH})$ values at an RH of 80%, which had an average value of 1.97 in this study, are extracted for comparison with other studies. When the RH was 80%, the aerosol particulate scattering coefficient was nearly 2 times that in dry conditions, which is relatively large compared with other studies (Liu et al., 2013b). Consequently, the RH contributed much more to aerosol extinctions in October 2014, leading to more severe hazes.

11003

Visibility dependences on the mass concentration of PM_{2.5} at different RH intervals are shown in Fig. 15 overall, the visibility decreased rapidly with increasing PM_{2.5} concentrations. In addition, with increasing RH, the visibility decreased faster. For example, when the RH was less than 30% and the mass concentration of PM_{2.5} was lower than 85 μg m⁻³, all of the visibilities were over 10 km. However, when the RH was greater than 90%, no visibility was more than 10 km in this observation. To quantify the relationship between visibility, the PM_{2.5} concentration and RH, Eq. (8) is used:

$$b_{\text{ext}}(\text{RH}) = b_{\text{sp}}(\text{RH}) + b_{\text{ap}} + b_{\text{sg}} + b_{\text{ag}}$$

$$= Q_{\text{sp}} \times \text{PM}_{2.5} \times \left(1 + a \times \left(\frac{\text{RH}}{100} \right)^b \right) + Q_{\text{ap}} \times \text{PM}_{2.5} + 34 \quad (9)$$

Where Q_{sp} and Q_{ap} are the mass scattering and absorbing efficiency, which are the ratios of b_{sp} and b_{ap} to PM_{2.5}, respectively. The average values of Q_{sp} and Q_{ap} in this study are 3.10 m² g⁻¹ and 0.42 m² g⁻¹. Curves of the dependence of visibility on the PM_{2.5} concentration at different RH intervals are shown in Fig. 15. The calculated curves showed the same trend as the dotted figure: the higher the RH was, the faster the visibility decreased as the concentration of PM_{2.5} increased. When the concentration of PM_{2.5} reached 75 μg m⁻³ (the national secondary standard of PM_{2.5}), the visibility surpassed 10 km only when the RH was lower than 60%. To control haze, keeping PM_{2.5} under the national second standard alone is sufficient.

In previous studies, a temperature decrease was often reported (Liu et al., 2013a). It not only deprived the dynamics of the PBL development but also resulted in less heat turbulence, which is unfavorable for pollutant dispersion. Moreover, negative aerosol radiation forcing (ARF) was always recorded, indicating the feedback mechanism between radiation and aerosol loading (Quan et al., 2014). However, in this study, even though the solar radiation was reduced during the haze episodes, the temperature was steady or even increasing over a longer temporal range (several days). Water vapor, a greenhouse gas, had a vital effect on the atmospheric thermal balance. The short-

11004

5 wave radiation from the sun is not absorbed by water vapor, but the long-wave radiation from the earth can be largely absorbed by it. As a result, even less solar radiation reached the earth's surface, and the radiation from the earth supplied increasing heat to the atmosphere with increasing RH. Increasing temperature accelerated the chemical
10 reaction rate of aerosols and aggravated the haze. This situation could also be found in the haze in January 2013, but little research has focused on the temperature variation. Figure 16 depicts how RH influenced the haze formation. Water vapor in the atmosphere played a vital role in the formation of haze, which can not only accelerate the chemical transformation of secondary pollutants but also lead to hygroscopic growth of
15 aerosols. Furthermore, as an important greenhouse gas, it absorbed surface radiation, altering the thermal balance of the atmosphere, which finally affected haze formation. RH in autumn is much higher than winter (Dong et al., 2013). It highly increases the rate of secondary reaction and hygroscopic growth. Thus, when only considering RH, with the same level of emission haze in autumn will be severer. However, in reality
larger quantity of emission and increasing RH in last decade in winter (Cheng et al., 2015) resulted in heavier haze in winter season.

4 Conclusions

Comprehensive measurements were conducted during the haze episode from 5 October to 2 November 2014. To clarify the formation mechanism of haze in Beijing, the
20 physical and chemical characteristics of aerosol and the relevant meteorology parameters were analyzed. The major conclusions are as follows:

1. Four distinct haze episodes occurred in October 2014 in Beijing, China. The highest concentration of $\text{PM}_{2.5}$ was $469 \mu\text{g m}^{-3}$ in Beijing, and the highest increasing rate of the concentration of $\text{PM}_{2.5}$ was $4.44 \mu\text{g m}^{-3} \text{h}^{-1}$. The haze originated from
25 the Northern China Plain (NCP), developing to the southwest and northeast directions.

11005

2. The concentration of SO_4^{2-} was lower than that of NO_3^- , but the oxidation rate of SO_2 to SO_4^{2-} was faster than that of NO_2 to NO_3^- . Sharp increases in the SNA fraction in PM_1 in the haze episode indicated that new formation of SNA contributed most to the formation of haze.

3. In total, 54, 26 and 57 fire points were found in Hebei, Henan and Shandong provinces, respectively. The air mass during the first haze episodes mainly came from the south and southeast, originating from these provinces. The sudden increase in the concentration of organic matter, Cl^- and BC before each haze period indicated the importance of biomass burning and transport in the haze formation
10 in October 2014.

4. NCP was dominated by a weak high-pressure system during haze episodes. Beijing city slowed the wind speed and disturbed the wind direction. Overall, the winds blew from the northwest, northeast, and southwest. The $\text{PM}_{2.5}$ concentrations were relatively high within the wind speed boundary: 1 m s^{-1} for wind from the northwest, 1.5 m s^{-1} for wind from the northeast and 3 m s^{-1} for wind from the southwest.
15

5. A distinct decrease in the PBL height was observed during the four haze periods, compressing the local pollutants closer to the surface.

6. The four haze episodes in October 2014 were characterized by higher RH. High RH influenced the haze formation in three ways: accelerating the chemical transformation of secondary pollutants, leading to hygroscopic growth of aerosols and altering the thermal balance of the atmosphere.
20

Acknowledgements. This work was supported by the National Natural Science Foundation of China (No. 41175018 and No. 41475113) and by special fund of State Key Joint Laboratory of
25 Environment Simulation and Pollution Control (No. 14L02ESPC).

- Miao, S., Chen, F., LeMone, M. A., Tewari, M., Li, Q., and Wang, Y.: An observational and modeling study of characteristics of urban heat island and boundary layer structures in Beijing, *J. Appl. Meteorol. Clim.*, 48, 484–501, 2009.
- 5 Miller, K. A., Siscovick, D. S., Sheppard, L., Shepherd, K., Sullivan, J. H., Anderson, G. L., and Kaufman, J. D.: Long-term exposure to air pollution and incidence of cardiovascular events in women, *New Engl. J. Med.*, 356, 447–458, 2007.
- Quan, J., Tie, X., Zhang, Q., Liu, Q., Li, X., Gao, Y., and Zhao, D.: Characteristics of heavy aerosol pollution during the 2012–2013 winter in Beijing, China, *Atmos. Environ.*, 88, 83–89, 2014.
- 10 Sun, Y. L., Zhuang, G. S., Tang, A. H., Wang, Y., and An, Z. S.: Chemical characteristics of PM_{2.5} and PM₁₀ in haze-fog episodes in Beijing, *Environ. Sci. Technol.*, 40, 3148–3155, 2006.
- Sun, Y. L., Wang, Z. F., Fu, P. Q., Yang, T., Jiang, Q., Dong, H. B., Li, J., and Jia, J. J.: Aerosol composition, sources and processes during wintertime in Beijing, China, *Atmos. Chem. Phys.*, 13, 4577–4592, doi:10.5194/acp-13-4577-2013, 2013.
- 15 Sun, Y. L., Jiang, Q., Wang, Z. F., Fu, P. Q., Li, J., Yang, T., and Yin, Y.: Investigation of the sources and evolution processes of severe haze pollution in Beijing in January 2013, *J. Geophys. Res.-Atmos.*, 119, 4380–4398, 2014.
- Tao, M., Chen, L., Wang, Z., Ma, P., Tao, J., and Jia, S.: A study of urban pollution and haze clouds over northern China during the dusty season based on satellite and surface observations, *Atmos. Environ.*, 82, 183–192, 2014a.
- 20 Tao, M., Chen, L., Xiong, X., Zhang, M., Ma, P., Tao, J., and Wang, Z.: Formation process of the widespread extreme haze pollution over northern China in January 2013: implications for regional air quality and climate, *Atmos. Environ.*, 98, 417–425, 2014b.
- 25 Wang, H., Xu, J., Zhang, M., Yang, Y., Shen, X., Wang, Y., Chen, D., and Guo, J.: A study of the meteorological causes of a prolonged and severe haze episode in January 2013 over central-eastern China, *Atmos. Environ.*, 98, 146–157, 2014.
- Wang, W., Maenhaut, W., Yang, W., Liu, X., Bai, Z., Zhang, T., Claeys, M., Cachier, H., Dong, S., and Wang, Y.: One-year aerosol characterization study for PM_{2.5} and PM₁₀ in Beijing, *Atmos. Pollut. Res.*, 5, 554, doi:10.5094/APR.2014.064, 2014.
- 30 Watson, J. G.: Visibility: science and regulation, *J. Air Waste Manage.*, 52, 628–713, 2002.
- Wen, L., Chen, J. M., Yang, L. X., Wang, X. F., Xu, C. H., Sui, X., Yao, L., Zhu, Y. H., Zhuang, J. M., Zhu, T., and Wang, W. X.: Enhanced formation of fine particulate nitrate at a rural site

11009

- on the North China Plain in summer: The important roles of ammonia and ozone, *Atmos. Environ.*, 101, 294–302, 2015.
- 5 Wu, D., Bi, X., Deng, X., Li, F., Tan, H., Liao, G., and Huang, J.: Effect of atmospheric haze on the deterioration of visibility over the Pearl River Delta, *Acta Meteorol. Sin.*, 21, 215–223, 2007.
- Xue, J., Griffith, S. M., Yu, X., Lau, A. K. H., and Yu, J. Z.: Effect of nitrate and sulfate relative abundance in PM_{2.5} on liquid water content explored through half-hourly observations of inorganic soluble aerosols at a polluted receptor site, *Atmos. Environ.*, 99, 24–31, 2014.
- 10 Yang, Y., Liu, X., Qu, Y., Wang, J., An, J., Zhang, Y., and Zhang, F.: Formation mechanism of continuous extreme haze episodes in the megacity Beijing, China, in January 2013, *Atmos. Res.*, 155, 192–203, 2015.
- Zhang, J. K., Sun, Y., Liu, Z. R., Ji, D. S., Hu, B., Liu, Q., and Wang, Y. S.: Characterization of submicron aerosols during a month of serious pollution in Beijing, 2013, *Atmos. Chem. Phys.*, 14, 2887–2903, doi:10.5194/acp-14-2887-2014, 2014.
- 15 Zhang, Z. Y., Zhang, X. L., Gong, D. Y., Quan, W. J., Zhao, X. J., Ma, Z. Q., and Kim, S. J.: Evolution of surface O₃ and PM_{2.5} concentrations and their relationships with meteorological conditions over the last decade in Beijing, *Atmos. Environ.*, 108, 67–75, 2015.
- Zhao, P., Zhao, X., Zhang, X., and Xu, X.: Long-term visibility trends and characteristics in the region of Beijing, Tianjin, and Hebei, China, *Atmos. Res.*, 101, 711–718, 2011.
- 20 Zhao, X. J., Zhao, P. S., Xu, J., Meng, W., Pu, W. W., Dong, F., He, D., and Shi, Q. F.: Analysis of a winter regional haze event and its formation mechanism in the North China Plain, *Atmos. Chem. Phys.*, 13, 5685–5696, doi:10.5194/acp-13-5685-2013, 2013.

11010

Table 1. Overview of the instruments involved in this study.

Instrument	Parameter	Manufacturer model
TEOM	PM _{2.5}	Thermo. Electron., RP1405F
Visibility meter	Visibility	Belfort 6000
Aethalometer	BC	AE33
Integrating nephelometer	Aerosol scattering coefficient	Ecotech, Aurora 3000
Wind speed/ Temperature/RH sensor	Wind speed, Temperature, RH	Vaisala, GMT220, HMP45
ACSM	The NR-PM ₁ species	/

11011

Table 2. The slopes of PM_{2.5} concentrations during the four haze episodes ($\mu\text{g m}^{-3} \text{h}^{-1}$).

	Episode 1 ($\mu\text{g m}^{-3} \text{h}^{-1}$)	Episode 2 ($\mu\text{g m}^{-3} \text{h}^{-1}$)	Episode 3 ($\mu\text{g m}^{-3} \text{h}^{-1}$)	Episode 4 ($\mu\text{g m}^{-3} \text{h}^{-1}$)
$r(\text{PM}_{2.5})$	4.03	4.44	4.16	2.00

11012

Table 3. The slopes of SOR and NOR during three haze episodes.

	Episode 2 (h^{-1})	Episode 3 (h^{-1})	Episode 4 (h^{-1})
$r(\text{SOR})$	5.63×10^{-3}	7.05×10^{-3}	6.22×10^{-3}
$r(\text{NOR})$	1.64×10^{-3}	4.5×10^{-3}	1.49×10^{-3}

11013

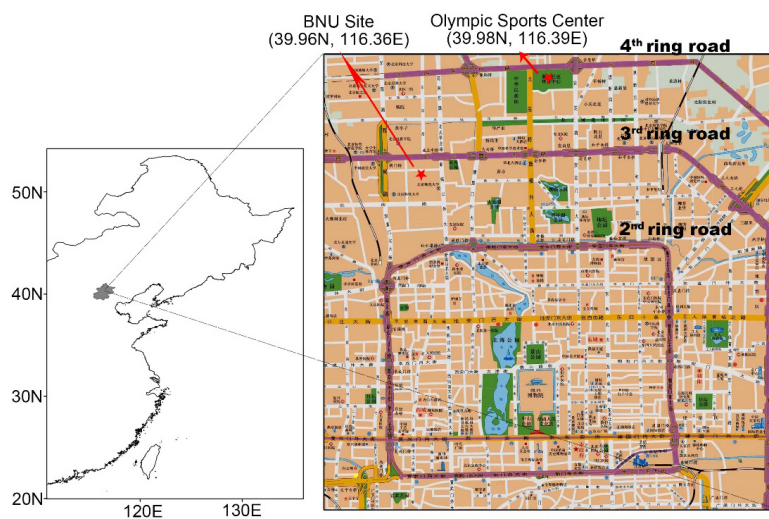


Figure 1. Observation sites in Beijing. All the data was obtained at BNU site except for gaseous pollutants, which were measured at Olympic Sports Center by National Environmental Bureau.

11014

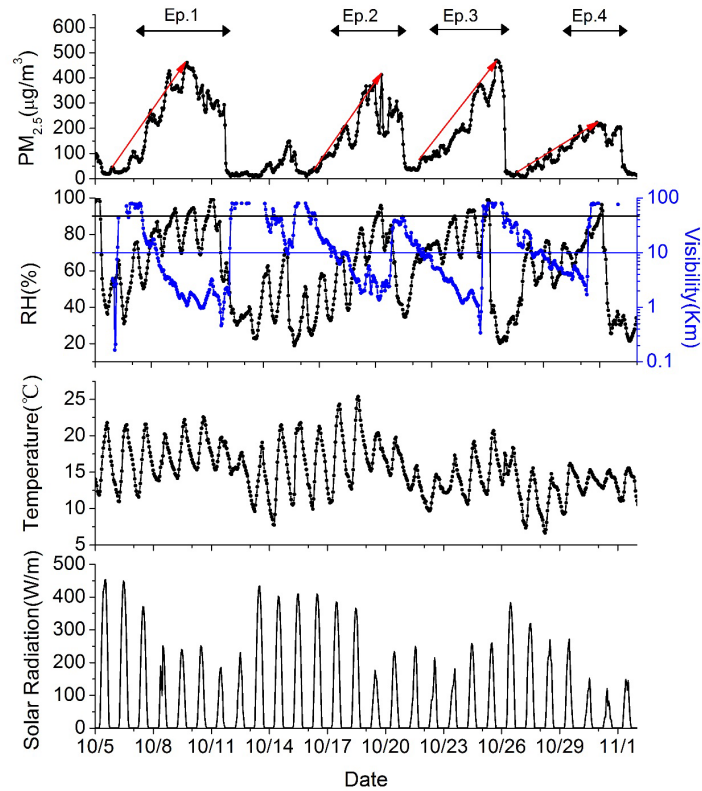


Figure 2. Time series of observed $PM_{2.5}$, RH, temperature and solar radiation in Beijing from 5 October to 2 November 2014.

11015

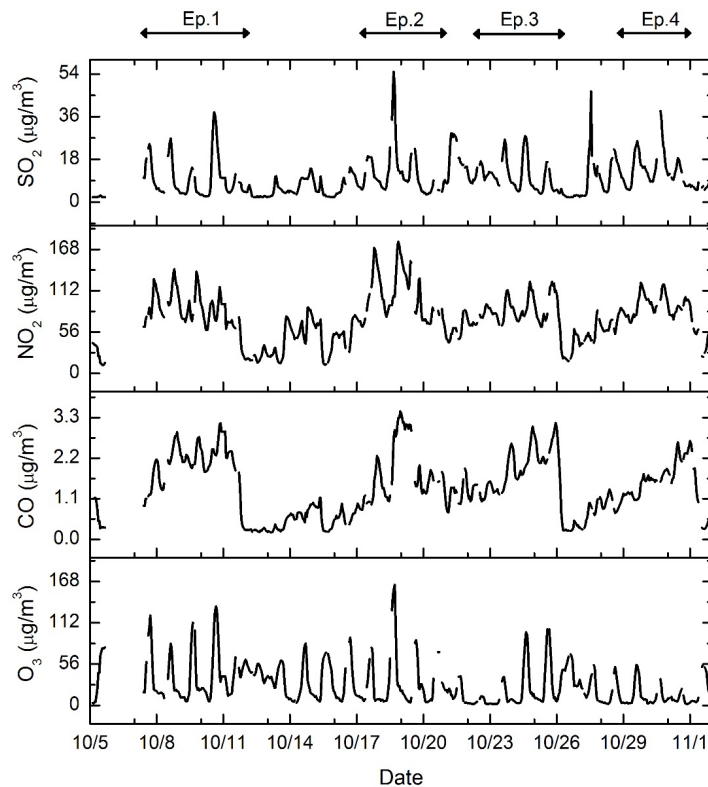


Figure 3. Time series of observed gaseous pollutants (SO_2 , NO_2 , CO , O_3) in Beijing from 5 October to 2 November 2014.

11016

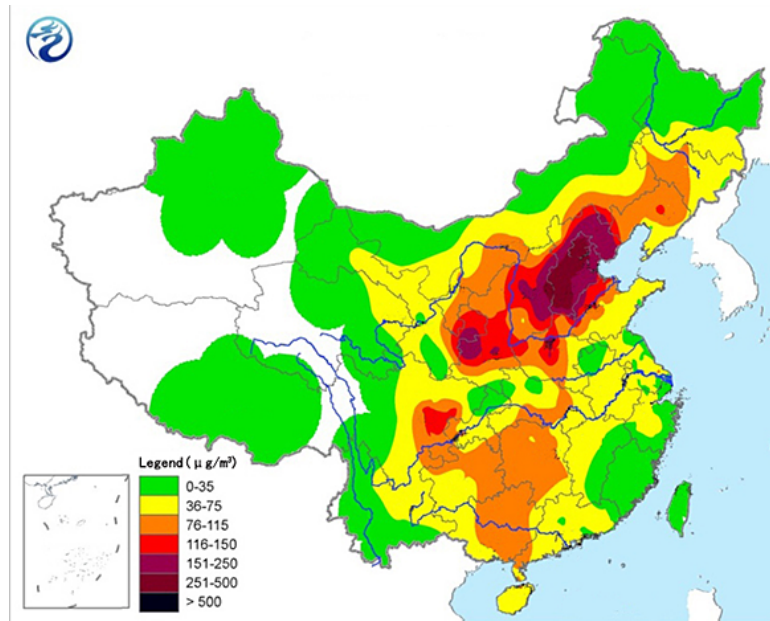


Figure 4. Spatial distribution of the PM_{2.5} concentration over China from 5 a.m. 9 October to 5 a.m. 10 October (from China Meteorological Administration, <http://www.nmc.gov.cn/publish/observations/environmental.htm>).

11017

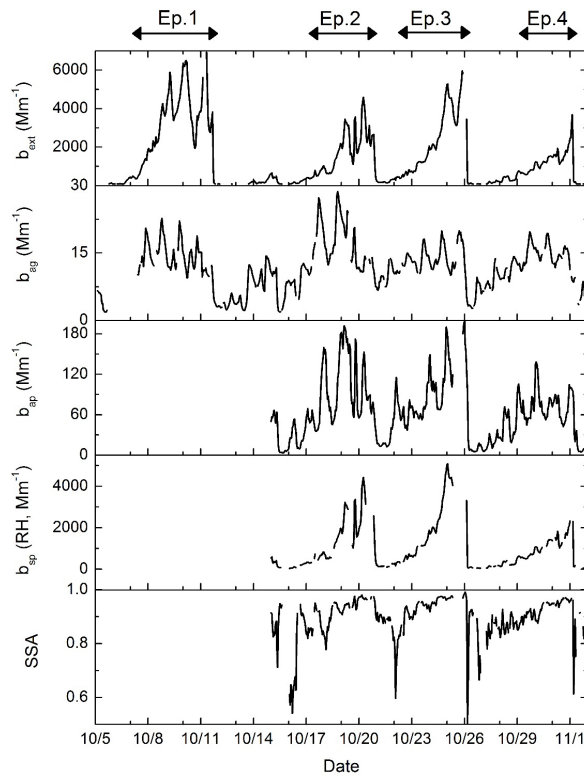


Figure 5. Time series of the atmospheric extinction coefficient b_{ext} , absorption by NO₂ coefficient b_{ag} , aerosol absorption coefficient b_{ap} , ambient aerosol scattering coefficient $b_{\text{sp}}(\text{RH})$, and single scattering albedo (SSA) in Beijing from 5 October to 2 November 2014.

11018

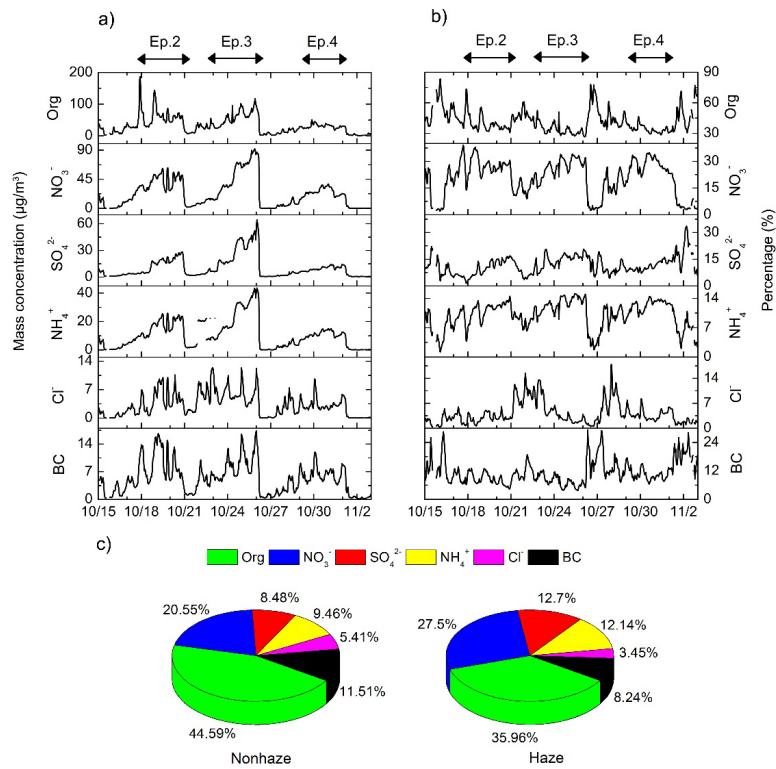


Figure 6. (a) Temporal variation of the mass concentration of each aerosol species in PM₁, (b) temporal variation of the mass fraction of each aerosol species in PM₁, (c) mass fraction of each aerosol species in PM₁ during non-haze and haze episodes from 15 October to 2 November 2014.

11019

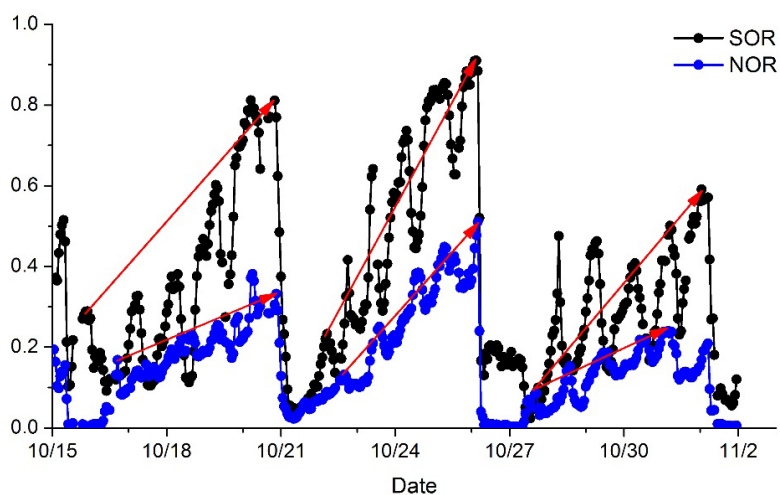


Figure 7. Time series of SOR (sulfate oxidation rate) and NOR (nitrate oxidation rate) from 15 October to 2 November 2014.

11020

Wind Vectors(KNTS) at Height: 10m AGL

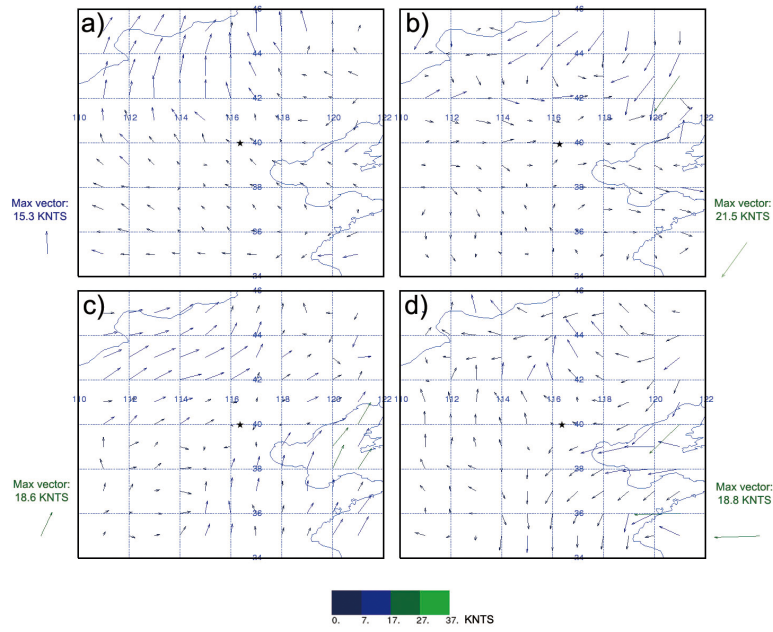


Figure 10. Wind field graphs of NCP at (a) 02:00, 10 October, (b) 02:00, 20 October, (c) 02:00, 24 October, and (d) 02:00 LST, 31 October; Black star denotes Beijing city, the color bar represents wind vectors.

11023

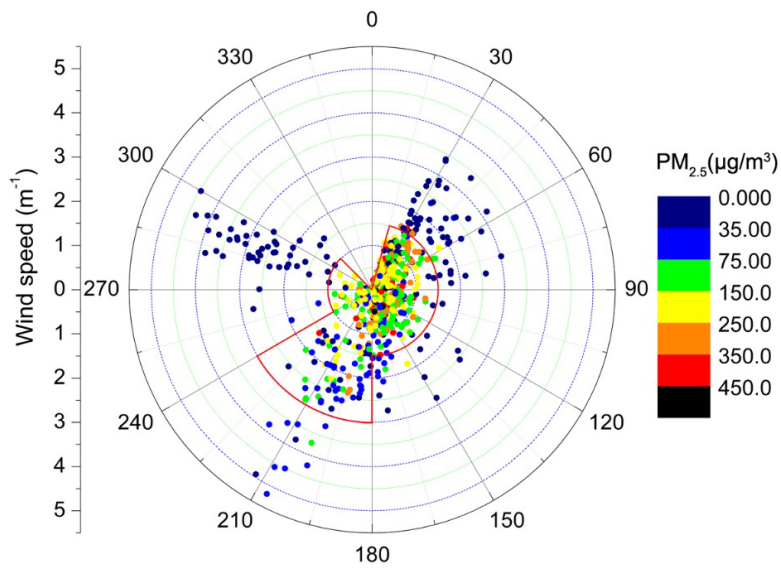


Figure 11. Wind rose diagrams of $PM_{2.5}$ in Beijing in October 2014.

11024

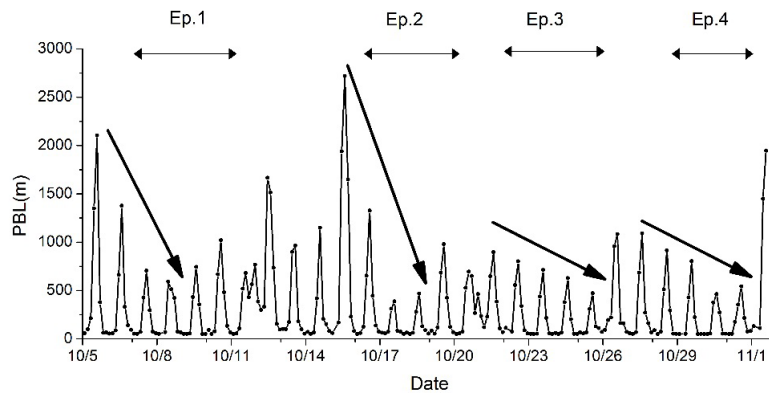


Figure 12. Time series of the PBL (planetary boundary layer) from 5 October to 2 November 2014.

11025

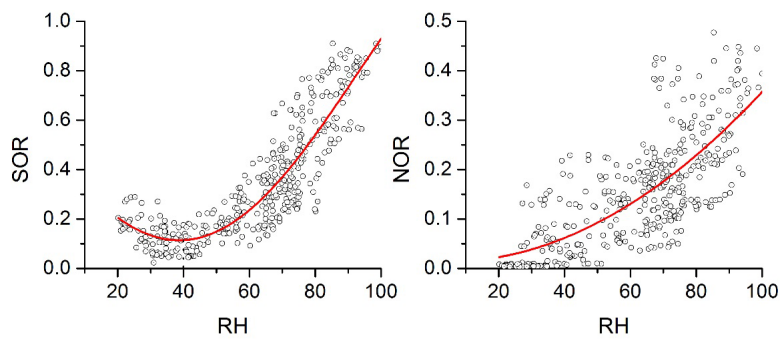


Figure 13. Relationship between RH (%) and SOR and between RH (%) and NOR during the haze episodes in October 2014.

11026

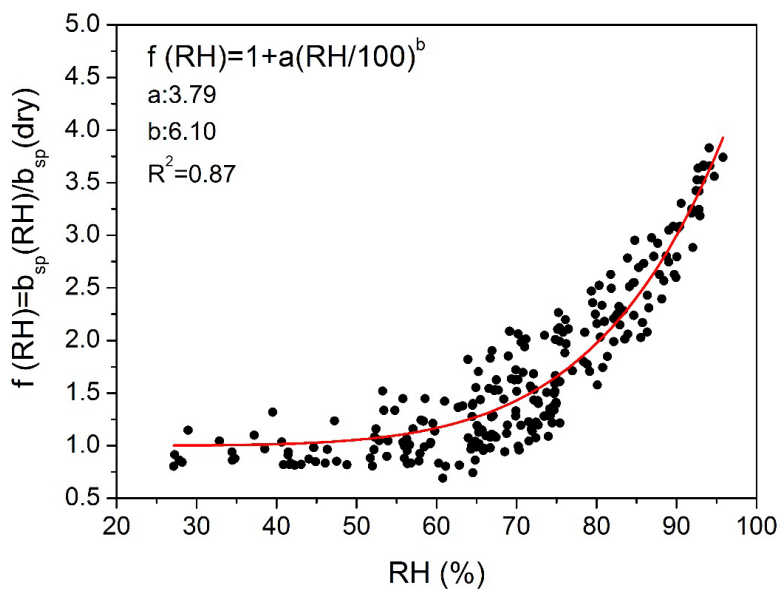


Figure 14. Hygroscopic growth for aerosol scattering $f(RH)$ as a function of RH with curve fitting. Scattered dots are the measured $f(RH)$ values, and the line is the empirical fitting curve.

11027

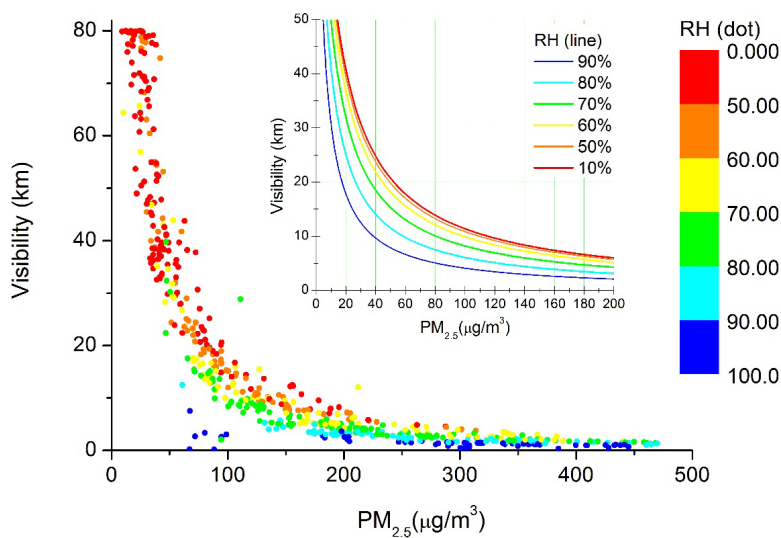


Figure 15. Variation of visibility at different RH values and different concentrations of $PM_{2.5}$, observed (dots) and simulated (lines).

11028

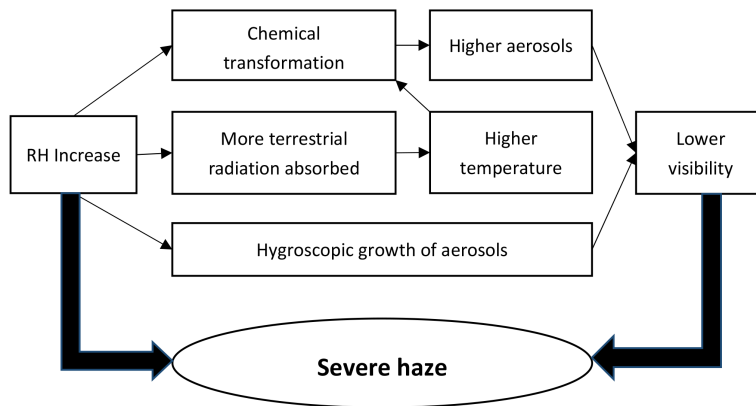


Figure 16. The mechanism of how RH influenced haze formation.